CANDU THREE-DIMENSIONAL NEUTRON-TRANSPORT CALCULATIONS WITH DRAGON

Wei Shen
Atomic Energy of Canada Limited
2251 Speakman Drive
Mississauga, ON, Canada L5K 1B2
shenwei@aecl.ca

ABSTRACT

Within the framework of adopting WIMS-AECL as the Industry Standard Toolset (IST) lattice-cell code for CANDU® analysis, it is imperative that a methodology compatible with this code be implemented for modelling the CANDU fuel bundle, reactivity devices, and fuel channels in three dimensions. The DRAGON code, developed and maintained at École Polytechnique de Montréal, Canada, has been recently selected as an IST code for CANDU three-dimensional (3-D) supercell transport calculations. The DRAGON neutron-transport code was designed for general geometry and can analyze CANDU fuel clusters, light-water reactor assemblies, and fast breeder reactor hexagonal assemblies in two dimensions. The code can also perform 3-D supercell neutron-transport calculations with the same group structures as those used in 2-D analysis. As an IST code, demand for the application of the DRAGON code to CANDU 3-D neutron-transport calculations is increasing. This paper summarizes some applications of DRAGON in CANDU-6 and ACR-700™ reactor-physics and fuel design.

1 INTRODUCTION

Through the Industry Standard Toolset (IST) project, the Canadian nuclear industry has selected three reactor-physics computer codes for use in safety analysis, licensing, and routine operations for CANDU nuclear reactors. These computer codes are WIMS-IST[1], RFSP-IST[2], and DRAGON-IST[3] (herein referred to as DRAGON). They are used for 2-D lattice-cell transport calculations, 3-D core analysis, and 3-D supercell transport calculations, respectively (note that DRAGON has been specifically selected for the calculation of the incremental cross sections for the reactivity devices in CANDU reactors only). The three IST reactor-physics codes fit together to create a calculational system for determining the neutron distribution in CANDU reactors.

The DRAGON neutron-transport code uses a 3-D multi-group formulation and solves the steady-state neutron-transport equation. The code was developed and is maintained at École Polytechnique de Montréal, Canada. It uses collision probability methods to set up and solve the neutron-transport equation in various spatial regions and in multiple neutron energy groups. DRAGON was designed for general geometry and can analyze CANDU fuel clusters, light-water reactor (LWR) assemblies, and fast breeder reactor (FBR) hexagonal assemblies in two dimensions. The code can also perform 3-D supercell neutron-transport calculations with the same group structures as those used in 2-D analysis. DRAGON has the capability to treat the self-shielding of resonance cross sections and to perform burnup

---

CANDU® is a registered trademark of Atomic Energy of Canada Limited (AECL).
ACR-700™ (Advanced CANDU Reactor™) is a trademark of AECL.

calculations. Several boundary condition options are provided, including standard infinite-lattice reflective boundaries, void-free boundaries, albedos, and periodic conditions. Thus, DRAGON can serve as a cell code, similar to WIMS-IST, APOLLO-2[4], CASMO-4, and HELIOS[5].

The main reason that DRAGON is part of the suite of IST reactor-physics codes is that DRAGON allows a good geometrical representation of the fuel bundles, reactivity devices, and fuel channels in 3-D, and that DRAGON's multigroup neutron-transport method is theoretically rigorous and consistent with WIMS-IST cell calculations. As an IST code, demand for the application of the DRAGON code to CANDU 3-D neutron-transport calculations is increasing. This paper summarizes some applications of DRAGON in CANDU-6 and ACR-700 reactor physics and fuel design.

Note that all the calculations reported in this paper were performed using the DRAGON code (version 3.03a, released as DRAGON981110) with the 89-group ENDF/B-V library. The results calculated with the latest released DRAGON (version 3.04), which is the IST version, give almost identical results as reported in this paper. Isotropic reflective tracking was carried out with the 3-D collision-probability module EXCELL of DRAGON. The transport equation was solved with a critical buckling search using the homogeneous B1 leakage method. The current standard ENDF/B-VI library was not used because it was unavailable in a format that the DRAGON code can use during the calculations.

2 MODELLING OF REACTIVITY DEVICES IN CANDU-6 AND ACR-700

The study of CANDU core performance requires the pre-calculation of few-group homogenized cross sections for CANDU lattice cells, and of incremental cross sections for in-core reactivity devices such as adjuster rods and liquid zone controllers (LZCs), which are located in the moderator, perpendicular to the horizontal fuel channels (see Figure 1). The reactivity-device incremental cross sections have to be derived from 3-D supercell calculations, which were previous calculated with the 3-D diffusion code MULTICELL[6]. To qualify DRAGON for CANDU applications, the DRAGON supercell methodology along with the RFSP-IST diffusion code have been evaluated against measurements made in the ZED-2 reactor, and in Phase-B commissioning tests in Pickering A Unit 4 and Darlington A Unit 4[7]. This section describes the DRAGON modelling of reactivity devices in current CANDU-6 and ACR-700 reactors.

2.1 SPECIFICATIONS OF CANDU-6 REACTIVITY DEVICES

CANDU-6 Lattice

The Point Lepreau reactor is used as the reference CANDU-6 reactor in this study. The typical CANDU-6 lattice, as shown in Figure 2, contains a 37-element natural-uranium (NU) bundle and pressurized heavy-water coolant in a pressure tube enclosed within a calandria tube. Surrounding this calandria tube, a 28.575-cm-square region of unpressurized heavy water at low temperature serves as the moderator.

Adjuster Rods, Mechanical Control Absorbers, and Shutoff Rods

There are 21 adjuster rods used in the Point Lepreau reactor, normally residing inside the core. Their main functions are to establish a flattened power shape and to override the negative xenon reactivity following reactor shutdown or power decrease. The adjuster rods are composed of stainless steel (SS) shim rods and SS tubes, and the adjuster-rod guide tubes are made of zircaloy-2. There are 4 mechanical

control absorbers (MCAs) and 28 shutoff rods (SORs), normally residing out of the core. Both the MCA and SORs are composed of a layer of cadmium sandwiched between two SS tubes. The MCAs and SORs guide tubes are made of zircaloy-2 and are perforated for moderator circulation. The SORs and MCAs are physically identical and only one type of MCAs/SORs is required for purposes of calculating the incremental cross sections. Note that the adjuster rods, MCAs, and SORs are all of annulus configuration.

Liquid Zone Controllers

The liquid zone controllers (LZCs) play an important role in the control of the 3-D core power distribution, especially for daily on-power refuelling. The LZCs are continuously emptied or filled with light water, upon request of the reactor regulating system. The 14 LZCs used in the Point Lepreau reactor are configured in 2 groups of 7 compartments. Each group consists of 3 devices, the central device having 3 compartments and the 2 outer devices having 2 compartments each (see Figure 3). The specification of the 3 compartment types depends on the number of feeder tubes (divided into concentric helium balance and light-water feeder tubes) and scavenger tubes (divided into concentric helium bubbler and light-water feeder scavenger tubes). The configuration of the central-top LZCs ("type 32", labelled 3 and 10 in Figure 3) is shown in Figure 4. Note that the configurations of the LZCs are more complex than those of adjuster rods, MCAs, and SORs.

2.2 SPECIFICATIONS OF ACR-700 REACTIVITY DEVICES

ACR-700 CANFLEX®-SEU Fuel Lattice

The typical ACR-700 CANFLEX-SEU lattice, as shown in Figure 2, contains a 43-element CANFLEX bundle and pressurized light-water coolant in a pressure tube enclosed within a calandria tube. Surrounding this calandria tube, a region of unpressurized heavy water at low temperature serves as the moderator. Compared with the current CANDU-6 lattice, the ACR-700 CANFLEX-SEU lattice is cooled with light water and has a smaller lattice pitch and a larger gap between the pressure tube and calandria tube[8]. The enrichment of the CANFLEX-SEU fuel used in this analysis is about 1.65 wt%.

Zone Control Rods and Shutoff Rods

Because of the small lattice pitch in the ACR-700 reactor, the reactivity devices were designed in the form of narrow oblong tubes. The zone control rods (ZCRs) are composed of SS, and the guide tubes are made of zircaloy-2. The shutoff rods, normally residing out of the core, are composed of a layer of cadmium sandwiched between two oblong SS tubes.

2.3 DRAGON 3-D SUPERCELL MODEL

The DRAGON modelling of the current CANDU reactivity devices can be found in Reference [9]. A typical supercell geometry used in the 3-D DRAGON models is illustrated in Figure 5. The supercell models were all of dimensions 2 lattice pitches x 1 lattice pitch x 1 bundle length, which is the normal supercell size given the device arrangement and symmetries in the reactor cores. The overall calculational strategy for the generation of reactivity-device incremental cross sections can be summarized as follows:

® CANFLEX is a registered trademark of AECL and the Korea Atomic Energy Research Institute (KAERI).

1) DRAGON 2-D cluster cell calculation in 89 energy groups;
2) Computation of 89-energy-group macroscopic cross sections using the 2D results;
3) Homogenization of the fuel-cladding-coolant region without energy condensation;
4) Approximation (e.g., annularization) of the reactivity devices, if necessary;
5) DRAGON 3-D supercell calculations with and without the reactivity devices; and
6) Calculation of 2-energy-group incremental cross sections using the difference between the previous 3-D results.

No approximations were made in the geometric modelling of adjuster rods and MCA/SOR with DRAGON. As DRAGON cannot treat either cluster or oblong geometry in 3-D, an annularization process was applied to represent the tubes inside the LZCs, and approximate rectangular geometries were used to represent the ZCRs and SORs in the ACR-700 reactor.

2.4 RESULTS

Table 1 summarizes the DRAGON-derived two-group incremental cross sections for empty light-water top-central ("type32") LZC in the Point Lepreau reactor. The one-and-a-half-group incremental cross sections derived from MULTICELL are also listed in Table 1 for reference. The RFSP-IST core calculations were performed with the simple-cell history-based method (SCM)[10] option for a typical core snapshot in a CANDU-6 reactor. The results in Table 2 indicate that the RFSP-IST-calculated reactivity worths with DRAGON-derived incremental cross sections are very comparable to the values calculated with WIMS-IST/MULTICELL-derived incremental cross sections. Compared with the WIMS-IST/MULTICELL-based values, the DRAGON-based reactivity worth is about 3% higher for LZCs, MCAs, and SORs, and is about 1% less for adjuster rods. Such differences between DRAGON- and WIMS-IST/MULTICELL-based reactivity worths are consistent with the validations of DRAGON supercell methods against commissioning tests in Pickering-A Unit 4 and Darlington-A Unit 4, which agreed to the measured values within about ±5% [7].

Table 3 summarizes the DRAGON-calculated lattice LZC reactivity worth and two-group incremental cross sections for different ZCR designs in the ACR-700 reactors. The lattice ZCR reactivity worth is defined as the change in the supercell reactivity due to the full presence of the ZCR, expressed as:

$$\Delta\rho(mk) = \rho(rodded) - \rho(unrodded) = 1000 \times \left(\frac{1}{K_{\infty}(unrodded)} - \frac{1}{K_{\infty}(rodded)} \right) \quad (1)$$

Note that the lattice ZCR reactivity worth reported here is calculated from lattice calculation assuming ZCR is presented in each bundle of the ACR-700 core, hence it is much larger than the real ZCR reactivity worth in the core. They are listed here just for design comparison purpose only. The real reactivity worth for ZCR should be calculated from RFSP-IST core calculation by using the two-group incremental cross sections listed in the table.

3 MODELLING OF CANDU-6 LIQUID ZONE CONTROLLERS IN THE UPPER REFLECTOR

The reactivity-device properties generated above can be used directly in the RFSP-IST code for the representation of reactivity devices and of structural materials in the core. Although these in-core properties have frequently been used to represent the devices in the reflector, it is an approximation because these properties are generated as incrementals to the fuel properties rather than to the reflector

properties and, when superimposed on reflector properties, they may result in non-physical local cross sections. However, for calculational simplicity, the properties derived from the in-core configurations were also used for adjuster-rod guide tubes, MCA guide tubes and SOR guide tubes in the reflector. Such approximations are considered to be suitable because the guide tubes are thin (no more than 0.15 cm thick) and are all made of Zircaloy-2 which has a very small neutron absorption cross section. Considering that the LZCs extend into the upper reflector, it is necessary to evaluate the accuracy of using these properties for the LZCs in the upper reflector.

3.1 DRAGON 3-D SUPERCELL MODEL

Clearly, only 6 of the 14 LZCs go through the upper reflector and have to be modelled separately with the DRAGON code: 2 central-top LZCs ("type 32", labelled 3 and 10 in Figure 3), 2 left-top LZCs ("type 21", labelled 1 and 8 in Figure 3), and 2 right-top LZCs ("type 21", labelled 6 and 13 in Figure 3). A typical supercell geometry used in DRAGON models for the central-top LZCs ("type 32") is illustrated in Figure 6. The supercell models were all of dimensions 2 lattice pitches x 5.4 lattice pitches x 1 bundle length (57.15 cm x 154.25 cm x 49.53 cm), which is a compromise between precision and calculational efficiency. Reflective boundary conditions were used at each surface of X and Z directions. A vacuum boundary condition was used in the +Y direction for the reflector outer boundary. An albedo boundary condition was used in -Y direction to make the supercell near critical (in our case, the albedo was selected as 1.04). The bottom 6 lattices, with fuel and calandria cylinders in the Z direction, represent the fuel core. The top 6 lattices represent the upper reflector. This 3-D Cartesian supercell was designed based on the physical layout of central-top LZCs ("type 32") in the Point Lepreau reactor.

3.2 RESULTS

The DRAGON-derived 2-group incremental cross sections for the empty light-water central-top LZCs ("type 32") in the upper reflector are also summarized in Table 1. Such properties are more theoretically rigorous because they are based on the exact geometrical representation of the LZCs in the upper reflector. The results in Table 1 show that the incremental yield cross sections, the incremental F-factors, and the incremental H-factors are zero as expected.

The DRAGON-derived incremental cross sections were then applied in the RFSP-IST calculations for the Point Lepreau reactor, to verify the LZC worths and channel-power distribution with the new LZC properties in the upper reflector. The results shown in Table 4 indicate that the calculated LZC worths with the new LZC model (with different LZCs properties in the upper reflector) are almost the same as the values calculated with the original LZC model (with identical LZCs properties as calculated in Section 2, in both the core and upper reflector). RFSP-IST core analysis also shows that the changes induced in the channel-power distributions with the new LZC model are also very small (less than 0.12%). The effect of the new LZC model on LZC worths and channel-power distribution is considered negligible. It is concluded that the use of the original LZCs model is considered appropriate.

4 MODELLING OF THE FUEL-BUNDLE END REGION IN CANDU-6 AND ACR-700

A CANDU-6 fuel channel contains 12 fuel bundles, each measuring about 50 cm in length. The region separating the fuel in two adjoining bundles in a channel is called the "end region"; typically, this is taken as the last 1 to 2 cm at each end of a bundle (see Figure 7). The thermal neutron flux is higher in the end region of the bundle than at the bundle axial mid-point because of the gap between bundles and because the end region of the bundle is made up of material with very low neutron absorption properties,

such as Zircaloy-4 and coolant. The thermal flux also peaks during refuelling at the free end of the last-inserted fresh bundle when the entire fuel-bundle string is temporarily shifted toward the downstream end of the channel. This bundle-coolant contact configuration results in a greater thermal flux peak than that in the normal bundle-bundle contact configuration, although it lasts for only a short period of time (usually about 10 min) and occurs in fresh bundles.

End-region flux peaking leads to a higher fission rate, and hence, higher heat production and higher temperatures in the end region of the fuel bundle. For accurate evaluation of fuel performance, the 3-D spatial power distribution in the CANDU fuel bundle, including the end region, was calculated with DRAGON for CANDU-6 and ACR-700 fuels.

The Point Lepreau ZTFU02 fuel type and the as-built CANFLEX-NU fuel used in the Point Lepreau reactor for the demonstration irradiation were chosen as the reference 37-element and CANFLEX-NU fuels in this analysis, respectively. The parameters used for the ACR-700 CANFLEX-SEU fuel are the same as those used in Section 2.2, except that the enrichment of the CANFLEX-SEU fuel used in this analysis is about 1.5 wt%.

4.1 DRAGON 3-D END-REGION MODEL

A typical supercell geometry (X-Z layout, right-half only) used in DRAGON models for 37-element fuel in bundle-bundle contact configuration is illustrated in Figure 8. The supercell is of dimensions 1 lattice pitch x 1 lattice pitch in the X and Y directions, respectively, and its dimension in the Z direction is more than 1 bundle length (about 70 cm long). Isotropic reflective boundary conditions were applied in the external surfaces of the supercell model, with symmetrical boundary conditions imposed at the surfaces with dotted lines, as shown in Figure 8. To obtain reliable axial flux distributions, fine axial meshes were imposed in the Z direction. The selection of the supercell size and the mesh spacing is a compromise between precision and computer memory allowance.

After the transport calculation of the 89-energy-group spatial flux distribution, a multi-region homogenization was performed to generate an ASCII file database in which the 2-group neutron flux, 2-group macroscopic cross sections, and the volume of each fuel region were saved. From this ASCII file database, the end-peaking factors can be generated.

4.2 RESULTS

Table 5 summarizes maximum fuel-end power-peaking factors (fuel-end power-peaking factor is defined as the ratio of the fuel-end linear power in element ring *i* to the bundle-average linear power) and absolute local linear powers at the fuel end (nominal bundle power 800 kW) for fresh 37-element, CANFLEX-NU, and ACR-700 CANFLEX-SEU fuels in bundle-bundle contact and bundle-coolant contact configurations. These results show that, for the same operating conditions, the maximum element linear power at the fuel end is lower in fresh CANFLEX-NU fuel or ACR-700 CANFLEX-SEU fuel than it is in fresh 37-element NU fuel, because of the 43-element design in CANFLEX fuel.

For fresh 37-element NU fuel and CANFLEX-NU fuel, the maximum linear power at the fuel end is about 15% higher in the bundle-coolant contact configuration than in the bundle-bundle contact configuration. In contrast, for fresh ACR-700 CANFLEX-SEU fuel, with light-water coolant the maximum linear power at the fuel end in the bundle-coolant contact configuration is only 8% higher than in the bundle-bundle contact configuration.

It should be noted that all the calculations were performed for fresh fuel because the most severe power peaking occurs during the refuelling transient when the coolant contacts the free end of the last-inserted bundle with fresh fuel or slightly irradiated fuel. The DRAGON prediction has been validated to have an uncertainty of ±1.3% for 37-element fuel[11]. There is no reason to expect that this margin of uncertainty would be degraded in CANFLEX fuel.

5 MODELLING OF THE FAST FLUENCE IN THE ENDPLATE OF THE CANDU FUEL BUNDLE

The fast fluence in the endplate of the CANDU fuel bundle, defined by the following equation, is an important fuel design parameter that is used for secondary stress analysis:

$$\Phi_{fast}^{endplate}(T) = \int_0^T \phi_{fast}^{endplate}(t)dt \tag{2}$$

where:

$\Phi_{fast}^{endplate}(T)$: time-dependent fast fluence in the endplate, n/cm^2

$\phi_{fast}^{endplate}(t)$: time-dependent fast flux (flux for neutron energy > 1 Mev) in the endplate, n/cm^2/sec

T: total time, sec

The calculation of the fast fluence is a complicated 3-D transport-depletion problem. For calculational simplicity, we assume that the ratio of the fast flux in the endplate to that in the pressure-tube/gap/calandria-tube mixture, *R*, is invariant with fuel burnup; this ratio was calculated with DRAGON for fresh fuel. The DRAGON 3-D end-region model outlined in Section 4 can be adopted as the reference for such calculation. The burnup-dependent fast fluxes in the pressure-tube/gap/calandria-tube mixture, $\phi_{fast}^{mix}(t)$, were calculated with WIMS-IST. Based on the assumption, the burnup-dependent fast flux in the endplate, $\phi_{fast}^{endplate}$, was thus generated by multiplying the above DRAGON-derived ratio *R* with WIMS-AECL-generated fast flux ϕ_{fast}^{mix}, i.e., $\phi_{fast}^{endplate} = R \cdot \phi_{fast}^{mix}$.

Figure 9 shows three typical CANFLEX-NU bundle power histories for (1) the nominal-design-power envelope, (2) bundle shifting from position 1 to 9, and (3) bundle shifting from position 2 to 10. Since higher power always produces higher fast flux (and hence higher fast fluence) for a given fuel bundle, use of the nominal design power envelope is considered more conservative as it is expected to produce higher fast fluence than that produced by using power histories for bundle shifts 1-9 and 2-10. Based on the nominal-design-power envelope shown in Figure 9 and in column 4 of Table 6, the bundle-burnup-dependent endplate fast flux, $\phi_{fast}^{endplate}$, and fast fluence, $\Phi_{fast}^{endplate}$, are summarized as a function of bundle burnup in columns 5 and 6 of Table 6 respectively.

CONCLUSION

The DRAGON code has been recently selected as an Industry Standard Toolset (IST) code for CANDU three-dimensional supercell transport calculations, as DRAGON allows a good geometrical representation of the fuel bundles, reactivity devices, and fuel channels in 3-D, and DRAGON's multigroup neutron-transport method is theoretically rigorous and consistent with WIMS-IST cell calculations. This paper presents several applications of DRAGON in CANDU-6 and ACR-700 reactor

physics and fuel design.

The applications include calculation of incremental cross sections for reactivity devices in the core, calculation of incremental cross sections for liquid zone controllers in the upper reflector, calculation of fuel-bundle end-region power peaking factors, and calculation of fast fluence in the endplate of the CANDU fuel bundle. It should be noted that the modelling of CANDU-6 shutdown system 2 with DRAGON is not included in this paper and will be reported later. For future applications, it is planed to use the latest DRAGON version 3.04 (method of characteristic is also available in this version) with the standard ENDF/B-VI library to perform more 3-D supercell calculations for CANDU-6 and ACR-700 reactors.

ACKNOWLEDGEMENTS

The DRAGON code was developed and is maintained at the Institut de Génie Nucléaire, École Polytechnique de Montréal. The author would like to express special thanks to Guy Marleau for his continuous advice and valuable suggestions in using the DRAGON code and its models in the past several years. The author is also grateful to J.V. Donnelly, H. Chow, D.A. Jenkins, P.S.W. Chan, and P. G. Boczar for useful technical discussions.

REFERENCES

1. J.D. Irish and S.R. Douglas, "Validation of WIMS-IST", *Proc. of 23rd Annual Conference of Canadian Nuclear Society*, Toronto, Canada, June 2-5 (2002).
2. M. Ovanes, D.A. Jenkins, et al, "Validation of the RFSP-IST Code Against Power-Reactor Measurements", *Proc. of 22nd Annual Conference of Canadian Nuclear Society*, Toronto, Canada, June 10-13 (2001).
3. G. Marleau, A. Hébert and R. Roy, "A User's Guide for DRAGON Version DRAGON_980911 Release 3.03", *IGE-174, Revision 4*, École Polytechnique de Montréal (1998).
4. R. Sanchez et al., "APOLLO-II: A User-Oriented, Portable, Modular Code for Multi-Group Transport Assembly Calculations", *Proc. of Int. Top. Mtg. Advances in Reactor Physics, Mathematics and Computation*, Paris, France, April 27–30 (1987).
5. E.A. Villarino, R.J.J. Stamm'ler, A.A. Ferri, and J.J. Casal, "HELIOS: Angularly Dependent Collision Probabilities", *Nucl. Sci. Eng.*, **112**, pp16 (1992).
6. A.R. Dastur and D. Buss, "MULTICELL—a 3-D Program for the Simulation of Reactivity Devices in CANDU Reactors", *AECL-7544*, Atomic Energy of Canada Limited (1983).
7. J.V. Donnelly and M. Ovanes, "Validation of 3-Dimensional Neutron Transport Calculations of CANDU Reactivity Devices", *Proc. of Int. Conf. On the Physics of Reactors(PHYSOR2000)*, Pittsburgh, USA, May 7-12 (2000).
8. P.S.W. Chan, K. Tsang, and D.B. Buss, "Reactor Physics of NG CANDU", *Proc. of 22nd Annual Conference of Canadian Nuclear Society*, Toronto, Canada, June 10-13 (2001).
9. R. Roy, G. Marleau, J. Tajmouati, and D. Rozon, "Modelling of CANDU Reactivity Control Devices with the Lattice Code DRAGON", *Ann. Nucl. Energy*, **21**, pp115-132 (1994).
10. J.V. Donnelly, "Development of a Simple-Cell Model for Performing History-Based RFSP Simulations with WIMS-AECL", *Proc. of Int. Conf. On the Physics of Nuclear Science and Technology (PHYSOR1998)*, Long Island, USA, October 5-8 (1998).
11. W. Shen, "Validation of DRAGON End-Flux Peaking and Analysis of End-Power-Peaking Factors for 37-Element, CANFLEX, and Next-Generation CANDU Fuels", *Proc. of 22nd Annual Conference of Canadian Nuclear Society*, Toronto, Canada, June 10-13 (2001).

Table 1. Incremental Cross Sections for the Empty Light-Water Central-Top LZCs ("Type 32") in the Point Lepreau Reactor (Equilibrium Core)

Property Type	WIMS-IST/MULTICELL (1.5 group $\Delta\Sigma$ in the Core)	DRAGON (2 group $\Delta\Sigma$ in the Core)	DRAGON (2 group $\Delta\Sigma$ in the Reflector)
$\Delta\Sigma_{tr1}$ (cm^{-1})	-1.41783E-2	-5.7708E-03	-1.5241E-02
$\Delta\Sigma_{tr2}$ (cm^{-1})	-8.2300E-3	-4.6224E-03	-7.5105E-03
$\Delta\Sigma_{a1}$ (cm^{-1})	-3.1200E-5	5.0962E-06	2.7299E-05
$\Delta\Sigma_{a2}$ (cm^{-1})	2.3140E-4	2.5925E-04	1.9339E-04
$\Delta\Sigma_{s1\rightarrow2}$ (cm^{-1})	-3.0250E-4	-1.8931E-04	-6.8450E-04
$\Delta\Sigma_{s2\rightarrow1}$ (cm^{-1})	0	-1.1804E-06	6.1186E-07
$\Delta\nu\Sigma_{f1}$ (cm^{-1})	0	-1.1430E-05	0
$\Delta\nu\Sigma_{f2}$ (cm^{-1})	2.4000E-5	5.4444E-05	0
ΔF	0	2.0306E-03	0
$\Delta H1$ (10^{-11}kW cm^2 s)	0	-5.5367E-04	0
$\Delta H2$ (10^{-11}kW cm^2 s)	1.2387E-3	2.7270E-03	0

Table 2. Comparison of Total Reactivity Worths in the Point Lepreau Reactor with DRAGON- and WIMS-IST/MULTICELL-derived Incremental Cross Sections (Equilibrium Core)

Device Type	Reactivity Worths (mk)	
	DRAGON-Derived $\Delta\Sigma_x$	WIMS-IST/MULTICELL-Derived $\Delta\Sigma_x$
21 Adjuster Rods	-16.21	-16.35
14 LZCs	-7.08	-6.92
4 MCAs	-10.43	-10.13
28 SORs	-78.40	-76.82

Table 3. DRAGON-Calculated Lattice ZCR Reactivity Worth and Incremental Cross Sections for ZCRs in ACR-700 Design (Equilibrium Core)

Design	1	2	3
Relative Rod Thickness Compared to Design 1	1.0	1.5	2.0
Lattice ZCR Reactivity Worth $\Delta\rho(mk)$	61	77	88
$\Delta\Sigma_{tr1}$ (cm^{-1})	5.2388E-03	7.5223E-03	9.5869E-03
$\Delta\Sigma_{tr2}$ (cm^{-1})	5.5275E-03	7.2316E-03	8.4960E-03
$\Delta\Sigma_{a1}$ (cm^{-1})	8.8871E-05	1.2571E-04	1.5795E-04
$\Delta\Sigma_{a2}$ (cm^{-1})	1.9517E-03	2.4690E-03	2.8242E-03
$\Delta\Sigma_{s1\rightarrow2}$ (cm^{-1})	-1.3298E-04	-1.9285E-04	-2.4765E-04
$\Delta\Sigma_{s2\rightarrow1}$ (cm^{-1})	2.9888E-05	3.8849E-05	4.5446E-05
$\Delta\nu\Sigma_{f1}$ (cm^{-1})	-4.5861E-06	-6.4370E-06	-8.1004E-06
$\Delta\nu\Sigma_{f2}$ (cm^{-1})	4.9045E-04	6.3139E-04	7.3321E-04
ΔF	1.2459E-02	1.5872E-02	1.8292E-02
$\Delta H1$ (10^{-11}kW cm^2 s)	-1.2911E-04	-1.8165E-04	-2.2905E-04
$\Delta H2$ (10^{-11}kW cm^2 s)	1.4413E-02	1.8561E-02	2.1560E-02

Table 4. Comparison of Point Lepreau LZCs Worths with the New LZC Model and the Original LZC Model (Equilibrium Core)

LZC Modelled	Reactivity Worths (mk)	
	New LZC Model	Original LZC Model
14 LZCs	-7.08	-7.05
Central-Top LZCs* (3/10)	-0.60	-0.60
Left-Top LZCs* (1/8)	-0.90	-0.91
Right-Top LZCs* (6/13)	-0.94	-0.95

*Note: During calculations, all other LZCs were kept at 50% full.

Table 5. DRAGON-Calculated Maximum End-Power Peaking Factors for Different Fuel Bundles in Bundle-Bundle Contact and Bundle-Coolant Contact Configurations (Fresh Core)

Fuel Type	Configuration	Maximum Fuel-End Power Peaking Factor	Maximum Linear Power at Fuel End (kW/m)*
37-Element NU	Bundle-Bundle Contact	1.252	56.3 (outer ring)
37-Element NU	Bundle-Coolant Contact	1.445	65.0 (outer ring)
CANFLEX-NU	Bundle-Bundle Contact	1.271	49.1 (inner ring)
CANFLEX-NU	Bundle-Coolant Contact	1.613	62.3 (inner ring)
ACR-700 CANFLEX-SEU	Bundle-Bundle Contact	1.312	50.6 (outer ring)
ACR-700 CANFLEX-SEU	Bundle-Coolant Contact	1.415	54.6 (inner ring)

*Note: Nominal design bundle power is assumed as 800 kW

Table 6. Time-Dependent Fast Flux and Fast Fluence in the Endplate of the CANFLEX-NU Fuel Bundle (Fresh Core)

No	Time, Full-Power Day	Bundle Burnup, MWd/Mg(U)	Bundle Power, kW	Fast Flux, 10^{13} n/cm^2/s	Fast Fluence, n/cm^2
1	0.00	0.00	778.96	4.069	0.00
2	3.48	145.90	783.53	4.118	1.225E+19
3	8.71	366.90	788.37	4.167	4.323E+19
4	13.63	576.70	792.17	4.209	9.229E+19
5	18.62	790.70	794.95	4.245	1.600E+20
6	23.57	1003.90	796.88	4.274	2.465E+20
7	29.45	1257.00	799.00	4.306	3.552E+20
8	35.34	1511.40	800.00	4.331	4.867E+20
9	41.62	1782.70	799.00	4.345	6.424E+20
10	49.08	2104.20	798.80	4.364	8.267E+20
11	57.22	2454.70	796.05	4.370	1.042E+21
12	65.68	2817.80	792.43	4.369	1.290E+21
13	74.93	3212.00	787.21	4.361	1.573E+21
14	84.92	3634.80	780.43	4.343	1.893E+21
15	95.75	4089.30	773.00	4.321	2.253E+21
16	106.99	4555.50	763.38	4.286	2.652E+21
17	118.18	5014.10	753.36	4.248	3.090E+21
18	131.35	5545.90	741.69	4.201	3.572E+21
19	144.93	6085.70	729.12	4.147	4.098E+21
20	160.01	6674.80	715.48	4.088	4.671E+21
21	176.65	7312.20	700.39	4.020	5.295E+21
22	195.29	8010.60	685.26	3.951	5.973E+21
23	212.92	8657.20	671.28	3.887	6.700E+21
24	232.23	9351.00	657.18	3.821	7.480E+21
25	251.61	10032.90	644.28	3.760	8.311E+21
26	270.62	10689.10	632.12	3.702	9.190E+21

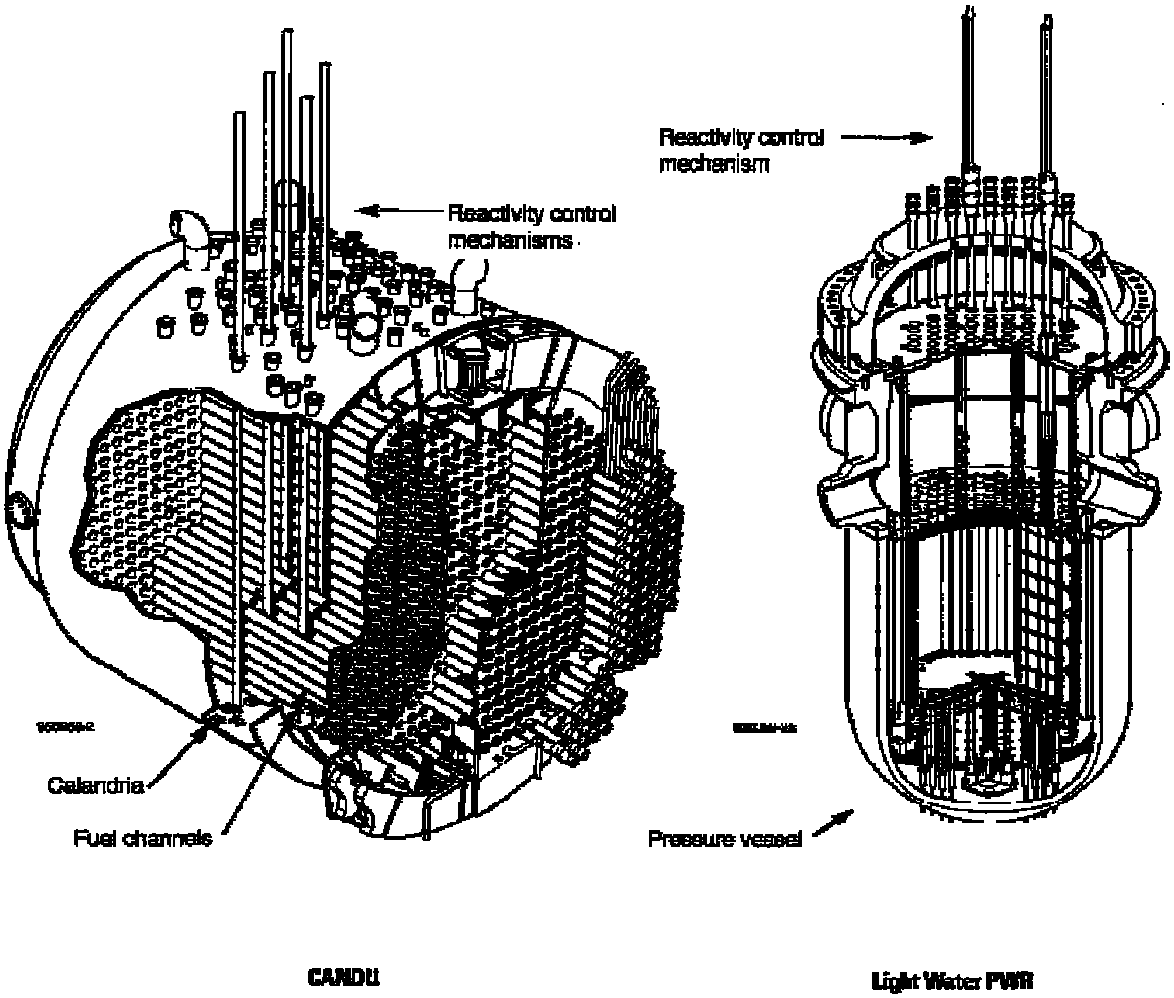

Figure 1. Layout of a CANDU-6 Reactor Compared with a PWR

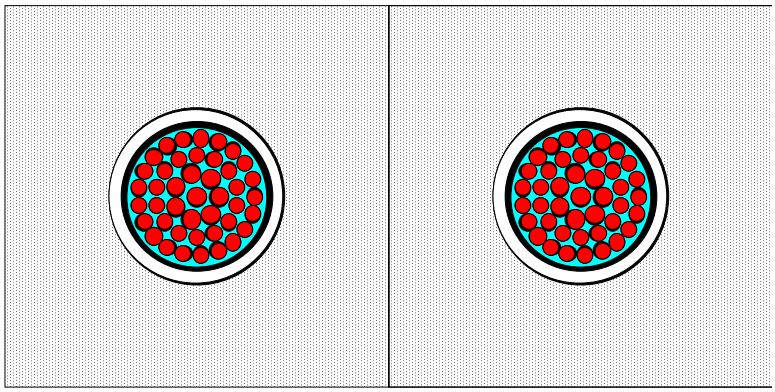

Two 37-Element NU Fuel Lattices

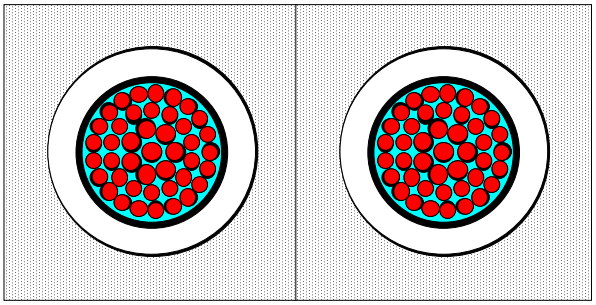

Two ACR-700 CANFLEX-SEU Fuel Lattices

Figure 2. Comparison Between CANDU-6 37-Element NU and ACR-700 CANFLEX-SEU Fuel Lattices

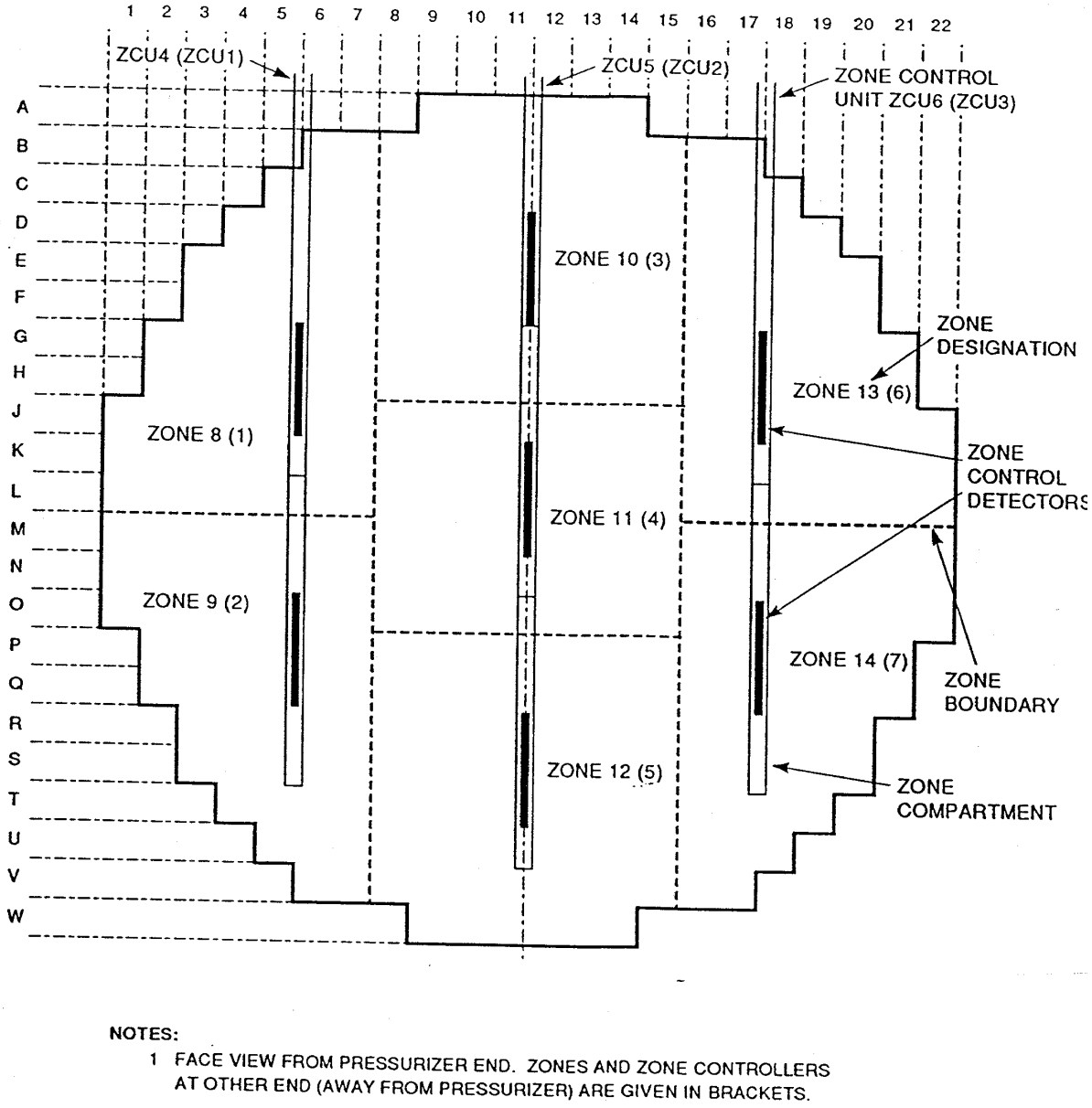

NOTES:

1 FACE VIEW FROM PRESSURIZER END. ZONES AND ZONE CONTROLLERS AT OTHER END (AWAY FROM PRESSURIZER) ARE GIVEN IN BRACKETS.

Figure 3. Vertical Locations of Point Lepreau Liquid Zone Controllers

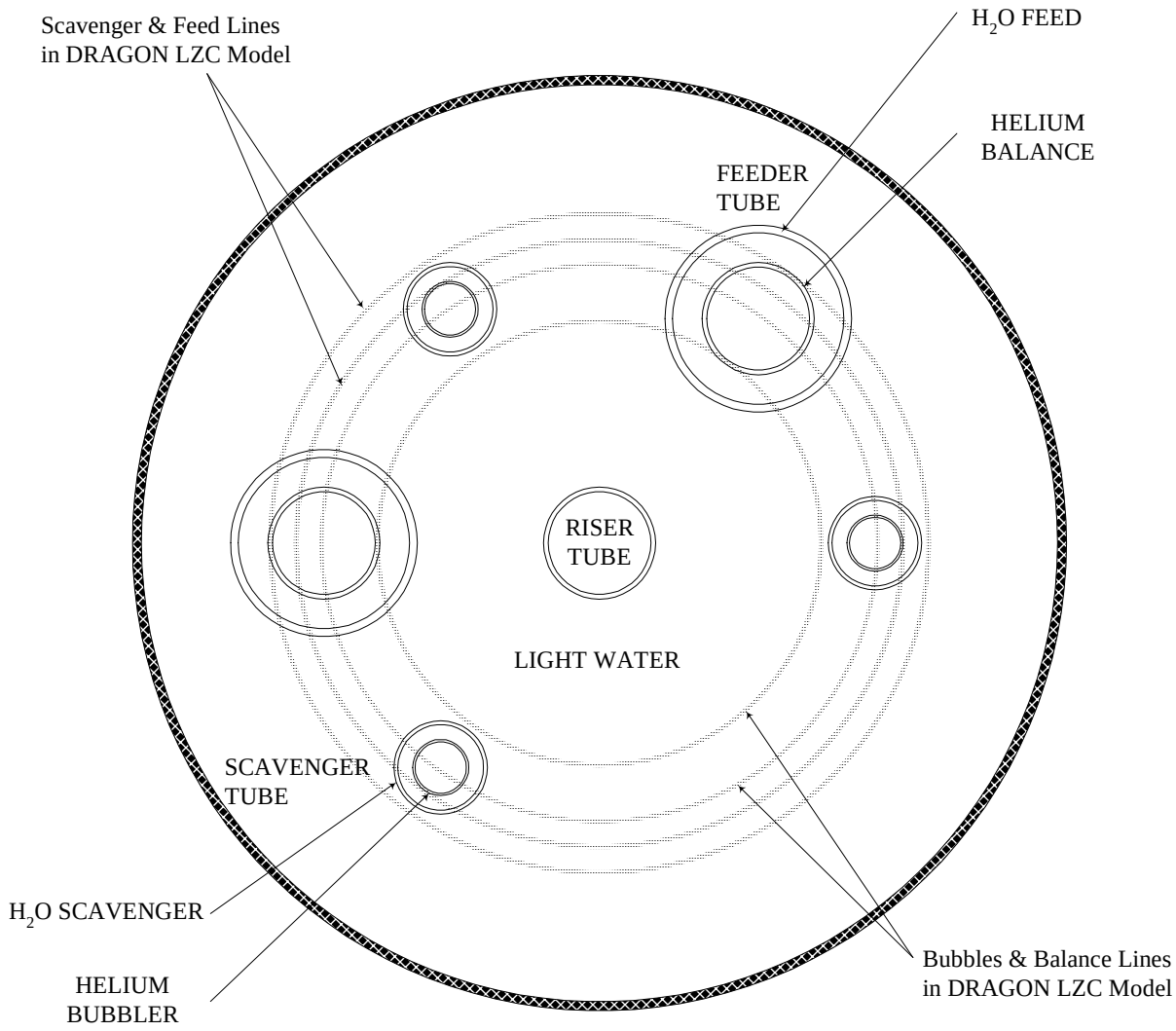

Note: The riser tube is located on the top of the calandria and does not extend into the core; therefore, it was not taken into account in the DRAGON model for zone controllers.

Figure 4. Typical Configuration of a Central-Top "Type 32" Liquid Zone Controller (Top View)

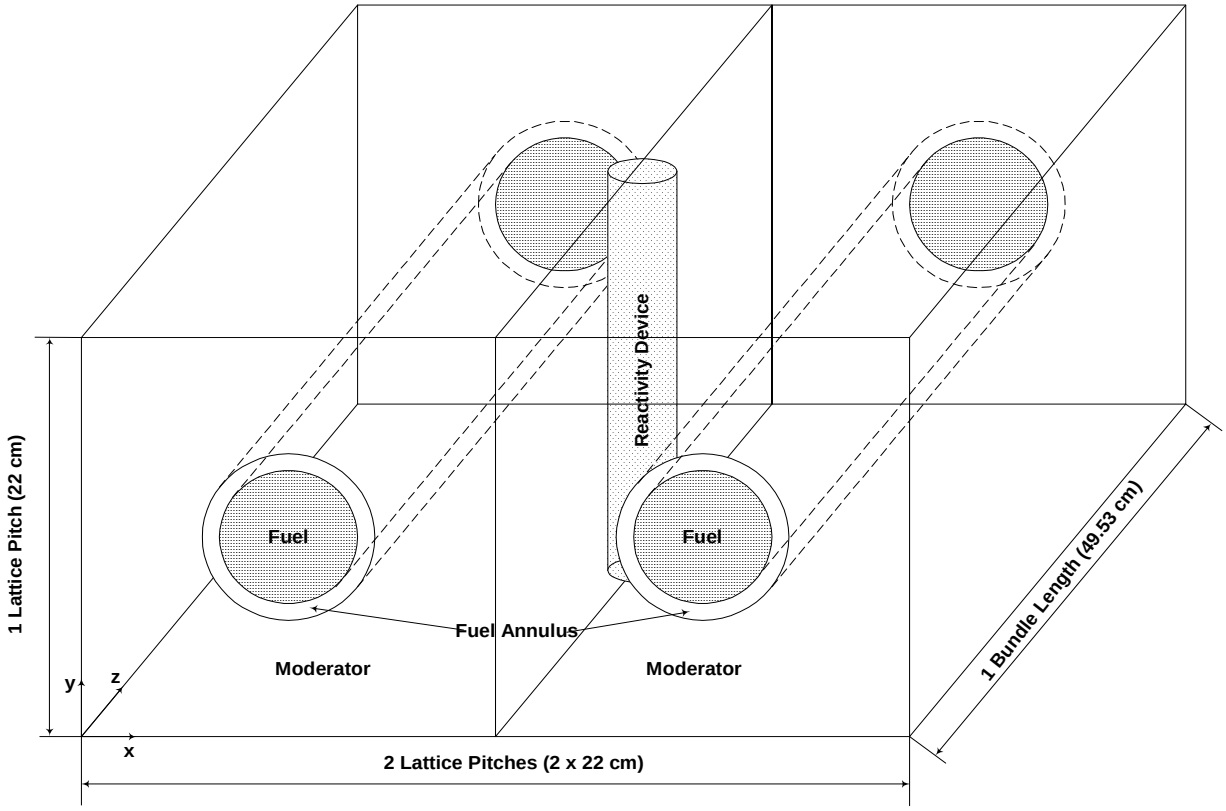

Boundary Conditions:

-x: Reflective +x: Reflective
-y: Reflective +y: Reflective
-z: Reflective +z: Reflective

Figure 5. A Typical 3-D Supercell Geometry with DRAGON

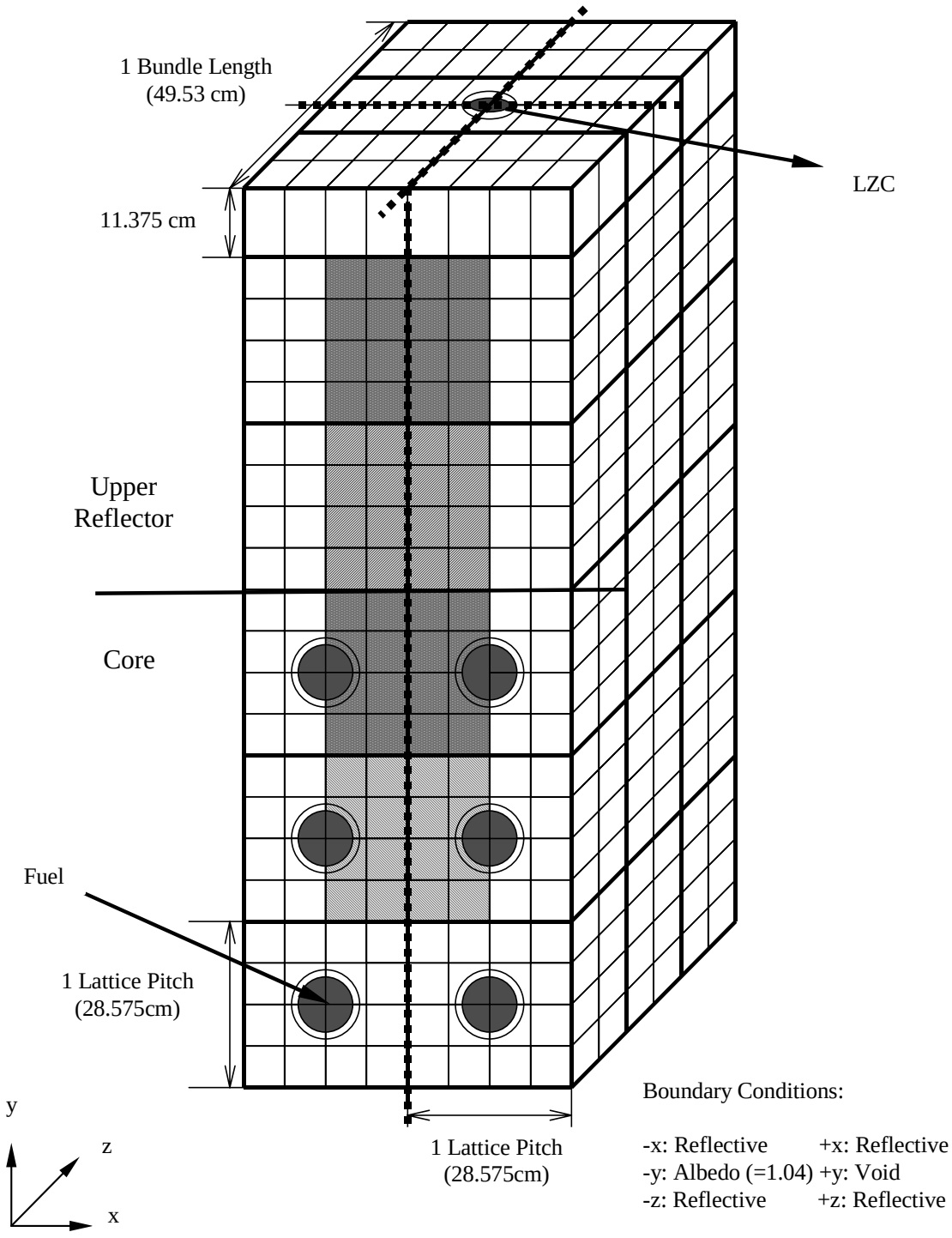

Figure 6. Supercell Modelling of a LZC in the Upper Reflector with DRAGON

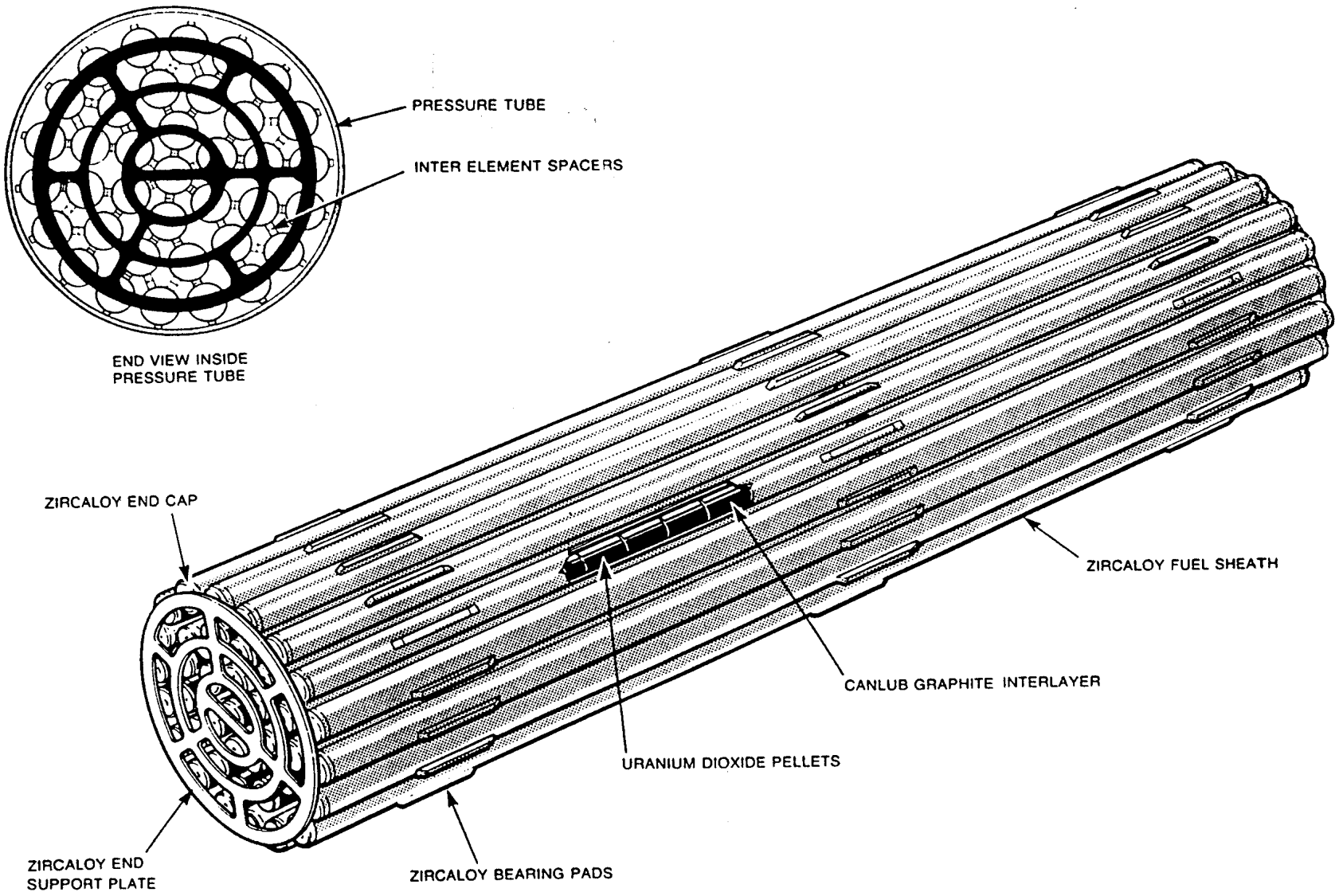

Figure 7. Schematic Representation of a CANDU-6 Fuel Bundle

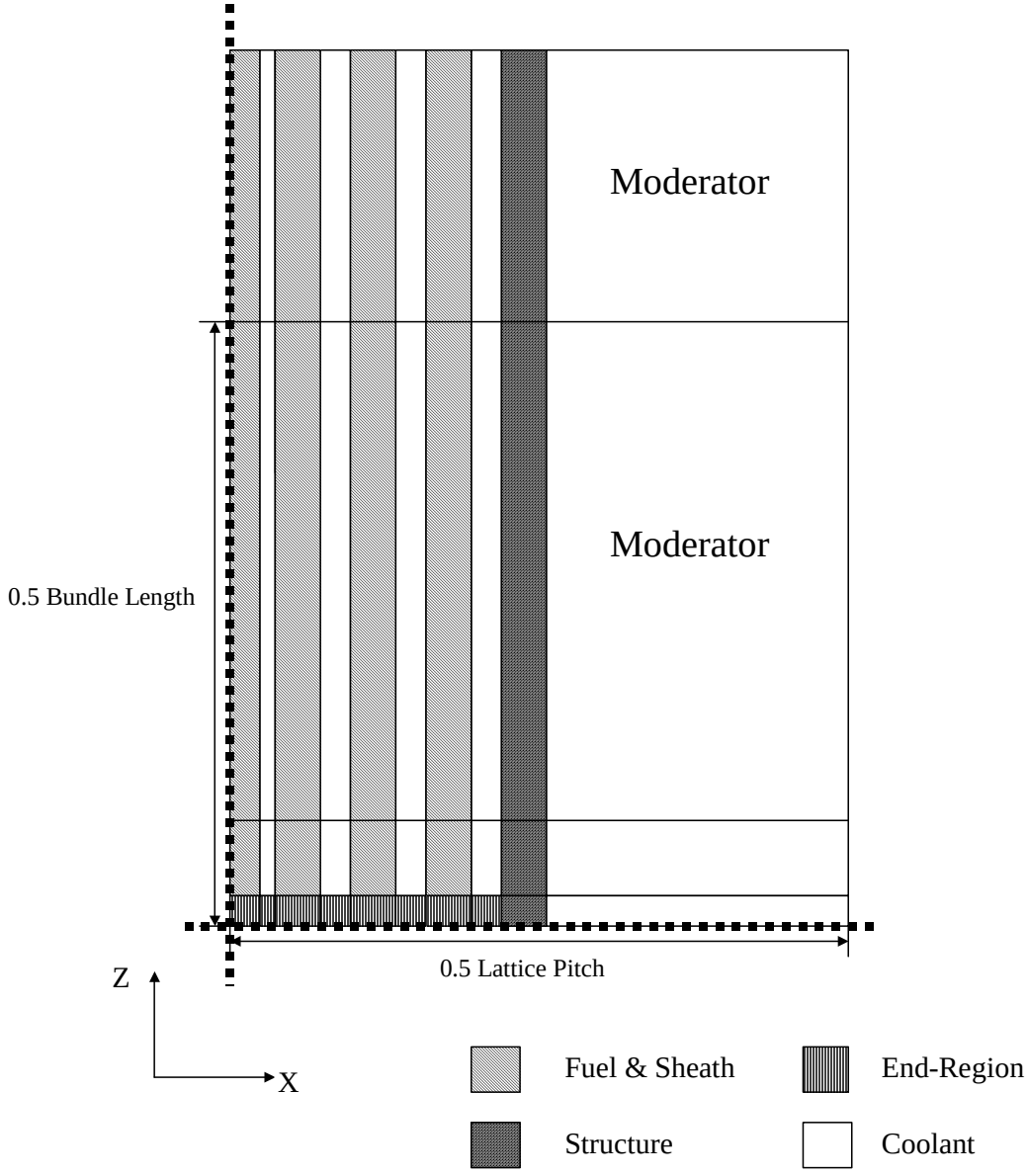

Figure 8. Supercell Modelling of End Region for 37-Element NU fuel, in Bundle-Bundle Contact Configuration (X-Z Layout, Right-half Only)

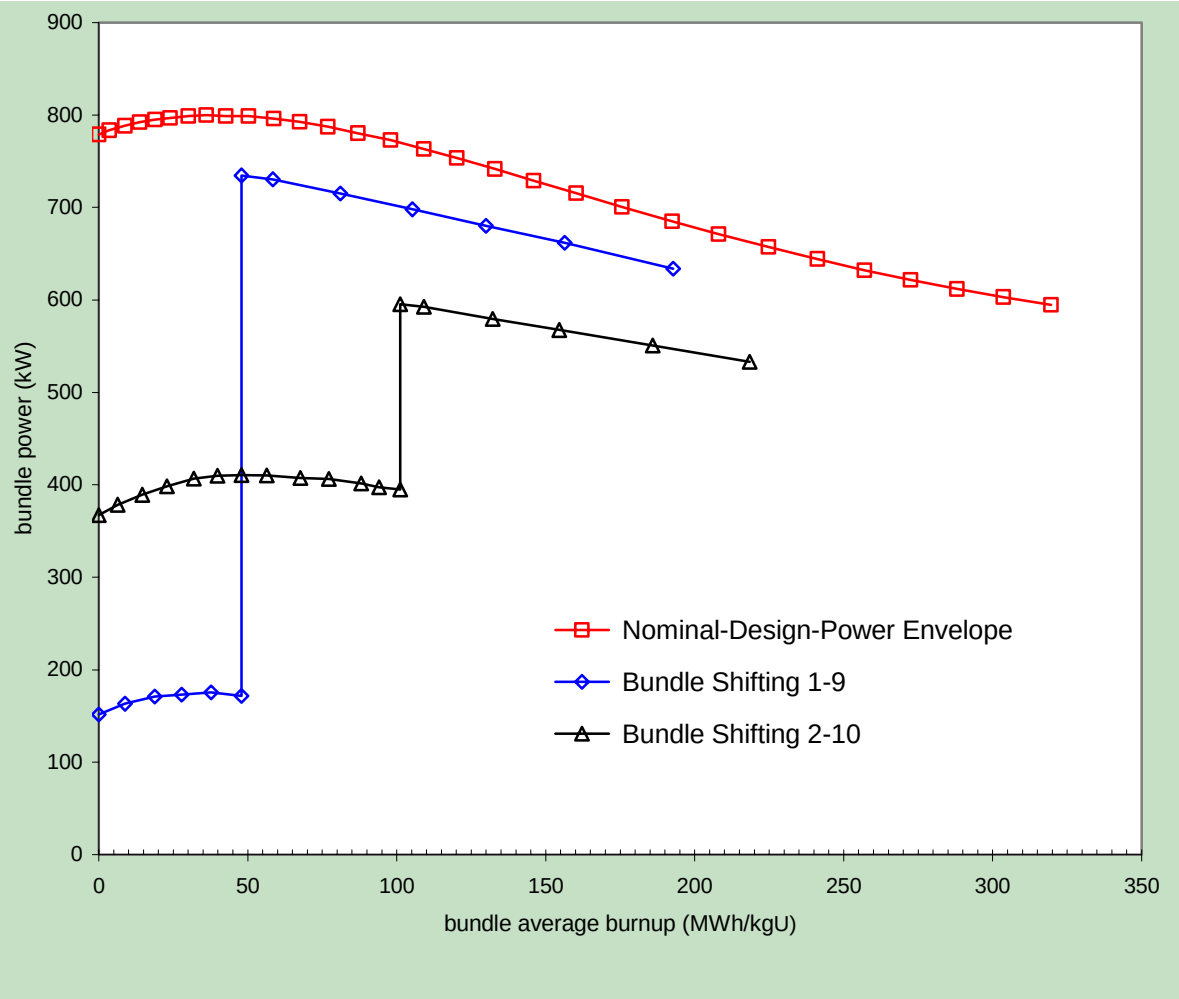

Figure 9. CANFLEX-NU Power Histories